

CubeSat single-photon detector module for investigating in-orbit laser annealing to heal radiation damage

Nigar Sultana,^{1,2,*} Joanna Krynski,^{1,3} Jin Gyu Lim,^{1,3} John Floyd,⁴
Michael Lembeck,⁴ Vadim Makarov,^{5,1,3} Paul Kwiat,⁴ and Thomas Jennewein^{1,3,6}

¹*Institute for Quantum Computing, University of Waterloo, Waterloo, ON, N2L 3G1 Canada*

²*Department of Electrical and Computer Engineering, University of Waterloo, Waterloo, ON, N2L 3G1 Canada*

³*Department of Physics and Astronomy, University of Waterloo, Waterloo, ON, N2L 3G1 Canada*

⁴*University of Illinois Urbana-Champaign, Champaign IL, United States*

⁵*Vigo Quantum Communication Center, University of Vigo, Vigo, Spain*

⁶*Quantum Information Science Program, Canadian Institute for Advanced Research, Toronto, ON, M5G 1Z8 Canada*

Single-photon avalanche photodiodes (SPADs) based on silicon are widely considered for quantum satellite communications but suffer from an increasing dark count rate (DCR) due to displacement damage in their active areas induced by proton radiation. When the DCR of SPADs exceeds a certain threshold, they become unusable for quantum communication protocols. Previous laboratory experiments have demonstrated that laser annealing of SPADs' active area with about 1 W optical power can significantly reduce radiation-induced DCR of synthetically irradiated SPADs. To assess the feasibility of in-orbit laser annealing on constantly irradiated SPADs in low-Earth orbit, we developed a module with a CubeSat form factor capable of both laser and thermal annealing of four silicon SPADs. Here we report the design and ground testing of this module, investigating laser annealing in a simulated space environment. Our results pave the way for an in-orbit trial that may prove this technology useful for future satellite missions with quantum receivers on board.

Keywords: Laser annealing, single-photon detectors, quantum communications, space instrumentation.

I. INTRODUCTION

Single-photon detectors (SPDs) are one of the key elements in satellite-based quantum communication networks [1–7]. These networks utilize SPDs either to detect received single photons in quantum receivers or to evaluate the performance of quantum sources in orbit. Quantum receiver satellites require SPDs with low dark count rate (DCR), low timing jitter, low afterpulsing probability, and high quantum detection efficiency at wavelengths suitable for optimal atmospheric transmission, such as at 800 nm [8, 9]. Commercial silicon-based single-photon avalanche photodiodes (SPADs) meet most of these requirements, with sufficiently high detection efficiency (above 60%) over a broad range of wavelengths (400–1000 nm). Si-SPADs have been successfully deployed in various space missions due to their long life, compact packaging, simple driving electronics, and modest cooling needs [10–13].

However, Si-SPADs are susceptible to damage from space radiation, particularly proton radiation with energies ranging from a few MeV to several hundred MeV [10]. The radiation-induced displacement damage leads to crystalline defects within the detector active regions, resulting in a constant increase in DCR, for example at a rate of approximately 30 counts per second per day, as observed at the Ice, Cloud, and land Elevation Satellite (ICESat) [10]. High DCR will degrade the implementation of quantum communication protocols, such as quan-

tum key distribution (QKD) [14, 15] and quantum teleportation [16], eventually making them impossible and thereby limiting mission lifetimes. To address this issue, previous ground studies have demonstrated the effectiveness of mitigating radiation-induced damage through thermal [17–23] or laser annealing [24, 25] procedures. Particularly, laser annealing using a controlled amount of laser light has been found to be more effective in reducing DCR by healing crystalline defects through focused heating of detector active areas [24]. However, the in-orbit effectiveness of laser annealing on continuously irradiated Si-SPADs in low Earth orbit (LEO) remains unknown. Therefore, our study aimed to develop technology for evaluating the efficacy of in-orbit laser annealing on continuously irradiated Si-SPADs, with the goal of extending mission lifetimes.

To facilitate this study, a detector (SPAD) module has been developed for the CubeSat mission CAPSat (Cool Annealing Payload Satellite) [26], and a similar design has been employed for the new satellite mission Space Entanglement and Annealing QUantum Experiment (SEAQUE) [27]. This paper presents a detailed design of our SPAD module, which enables thermal and laser annealing and detector characterization in orbit. The module employed a novel approach to fiber-coupling the annealing lasers to the SPADs, ensuring full illumination of the detector active areas. We demonstrated the module's operation in a simulated space environment inside a thermal vacuum chamber (TVAC), representing a significant step toward establishing in-orbit laser annealing of SPADs. This paper also presents performance test results for the detectors from the flight SPAD module and for laser-annealed irradiated detectors from an equivalent

* nigareipu@gmail.com

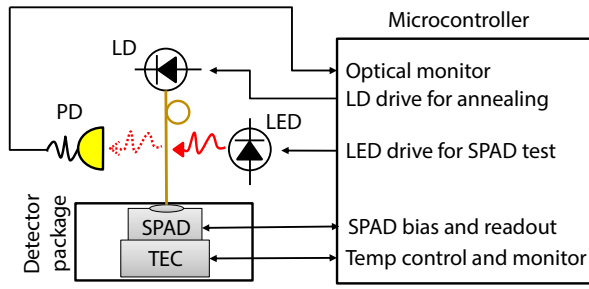


FIG. 1. Concept of the in-orbit laser annealing. A high-power beam from a laser diode (LD) is transmitted through an optical fiber and focused onto the active area of a SPAD. A light emitting diode (LED) acts as a reference light source for testing the detectors' photon detection efficiency. A photodiode (PD) is used to monitor the optical power from the LED; a thermoelectric cooler (TEC) integrated with the SPAD is employed for temperature regulation during operation, and a microcontroller controls the operation of all the devices.

flight-compatible engineering detector module.

II. MODULE DESIGN

A functional representation of an in-orbit laser annealing system is illustrated in Figure 1. The system employs a high-power annealing laser diode (LD) to illuminate SPAD active areas through an optical fiber. For verification of photon-detection efficiency, an adjacent light-emitting diode (LED) is used to emit light, which leaks into the jacketed fiber, primarily targeting the core of the fiber. The power output of the LED is monitored and measured using an additional photodiode (PD). The operation of all the components is intended to be controlled by a microcontroller (MCU). The MCU is also expected to collect telemetry data during in-orbit operations. This telemetry includes various metrics such as detector dark counts, temperature readings, TEC current, PD photocurrent, and other relevant measurements. Data collection can occur under different cooling temperatures, before and after each annealing cycle, and following a number of orbital revolutions, which can vary depending on the dark count (DCR) accumulation rate. The collected telemetry is subsequently transferred to the onboard computer for storage, until it can be transmitted to a ground station. Comprehensive experimental laser annealing protocols in terms of annealing laser power, annealing duration are analyzed in [28].

The laser annealing system built for the CAPSat is divided into two modules. The detectors and their associated circuitry required for performing in-orbit laser annealing and thermal annealing are housed in the SPAD module, while the other essential components for the annealing operation—such as the fiber-pigtailed LDs, LEDs, PDs, and the MCU—are located in a separate module known as the control module. Figure 2 illustrates the two integrated modules of the CAPSat annealing sys-

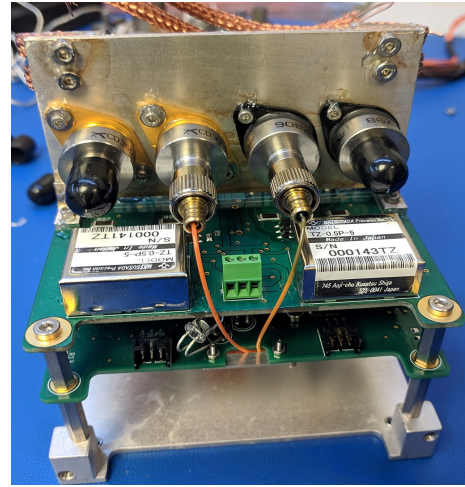


FIG. 2. SPAD module integrated with the CAPSat control module.

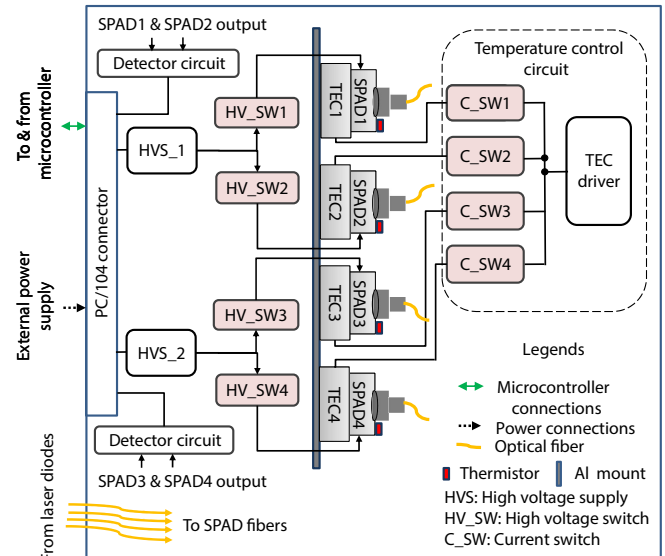


FIG. 3. Schematic overview of the CAPSat SPAD module, highlighting the main components and functional elements.

tem. This paper focuses solely on the SPAD module and provides its detailed design and performance results.

The SPAD module consists of two Excelitas SLiK and two Excelitas C30902SH detectors, each with active area diameters of $180\ \mu\text{m}$ and $500\ \mu\text{m}$, respectively. This module also includes detector biasing, quenching, pulse shaping and temperature control circuitry, a schematic overview is illustrated in Fig. 3. Each detector package, along with a SPAD, also includes a built-in two-stage thermoelectric cooler (TEC) and a thermistor used for detector temperature control and monitoring. The detectors are customized to have an attached fiber connector through which annealing lasers can be coupled via a multimode optical fiber, ensuring effective illumination of the entire active area. In CAPSat, only one SLiK and

one C30902SH detectors are fiber-coupled with a core diameter of $105\ \mu\text{m}$ with the two laser diodes of the control module for laser annealing, while the other two detectors from each variant remain as control devices that do not undergo laser annealing and are intended to measure the overall damage caused by space radiation.

The detectors are mounted on an aluminum plate, which serves as both a physical support and a heat sink. This plate is vertically attached to the module printed circuit board (PCB), which also holds two high-voltage supplies (HVS) to provide bias voltages, and two detector circuits consisting of quenching and pulse-shaping electronics for processing avalanche signals. Each circuit is shared by two SPADs. Only one SPAD is selectively activated during operation via a high-voltage switch (HV_SW, Panasonic Electric Works AQV216SX). Additionally, the PCB incorporates a TEC driver and four current switches (C_SW, Omron Electronics G3VM-21HR) to selectively control the current flow through one of the four TECs to maintain desired detector temperatures. This approach provides the flexibility to operate a single detector and a corresponding TEC at any given time, effectively minimizing the power consumption of the SPAD module. The power and control signals for the SPAD module are supplied from the control module via a PC/104 connector. At the development and testing phase of this module, a Cypress controller (CY8CKIT-030 PSoC) was used to supply the control signals.

The detectors of the SPAD module operate in Geiger mode [29] above the breakdown voltage V_b , generating an avalanche current in response to a single photon. This current is halted by a passive quenching circuit that includes a quenching resistor R1 or R2 of $402\ \text{k}\Omega$ [30], as shown in the detector circuit in Fig. 4(a). A digital-to-analog converter (DAC) internal to the MCU provides a control voltage ranging between 0–2.5 V for the HVS that outputs biasing voltages ranging between 0–500 V. When a SPAD is biased, each detection event creates a voltage drop across R3 ($100\ \Omega$), the magnitude of which is compared with a MCU-DAC-provided predefined threshold voltage (THR) using a high-speed radiation-tolerant comparator (DISC, STMicroelectronics RHR801). As the module supports only single-polarity supplies instead of the comparator’s requirement of dual-polarity power supply, the inputs must be within a range of 0.5–2.1 V with the use of $V_{CC} = +3.3\ \text{V}$ supply. Therefore, a reference of 900 mV is used instead of ground, using a voltage reference IC (Intersil ISL21070). When the voltage across R3 is higher than the predefined threshold, the comparator generates 3 V output pulses of 5–10 ns width. Their width is then increased to approximately 100 ns using a D flip-flop (D-FF; Texas Instruments 74AC11074pwr) so that they can be read out by the relatively slow MCU. A counter configured in the MCU then records the number of detection events within a measurement time period.

In order to minimize dark counts, and maintain a consistent detection efficiency at a fixed bias voltage, the SPADs are typically cooled to a fixed temperature, which

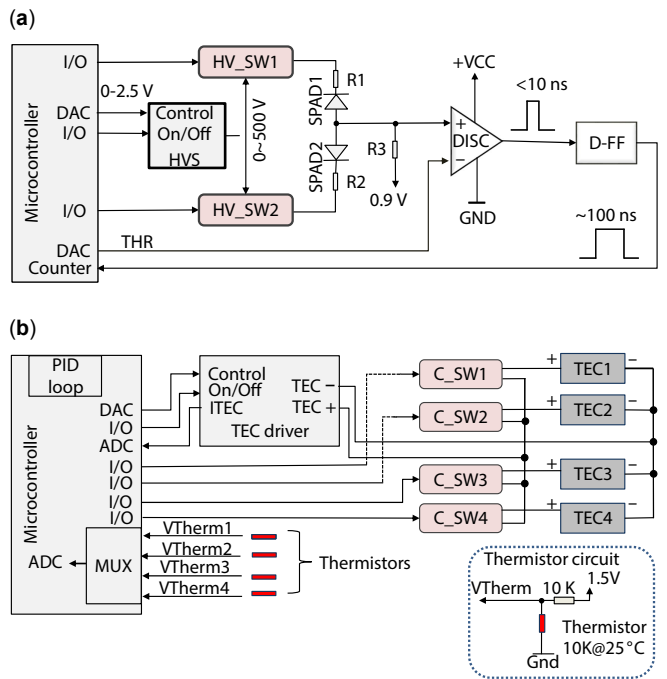


FIG. 4. Simplified circuit diagrams of detector electronics. (a) Detector biasing and quenching electronics. Two detectors share the same high-voltage supply (HVS) and passive quenching and pulse-shaping circuits. A microcontroller (MCU) controls HVS output, detector activation one at a time, discriminator threshold voltage, and records detector counts. (b) Temperature control circuits. A driver controls current flow and its direction through the TECs using feedback from a PID loop running on the MCU based on thermistor readings. The microcontroller activates one TEC at a time, reads thermistor values, and sends control signals to the TEC driver.

is controlled using their built-in TECs. The latter can also be utilized for thermal annealing by reversing the direction of the TEC current [Fig. 4(b)]. To control the current flow and direction through the TECs, a compact TEC driver (Maxim Integrated MAX1968) is employed, which receives feedback from a proportional integral derivative (PID) loop programmed in the MCU. The PID algorithm reads the instantaneous detector temperatures as a voltage drop across the built-in thermistors (V_{Therm}) via an MCU analog-to-digital converter (ADC). Based on the difference between the instantaneous and desired temperatures, the PID algorithm sends appropriate control voltages to the TEC driver to adjust its output current, which flows through the active TEC. The current flow is monitored by observing the ITEC readout of the TEC driver using the MCU ADC.

III. PERFORMANCE TESTS

Pre-radiation SPAD performance test: This test was performed at atmospheric pressure on the flight

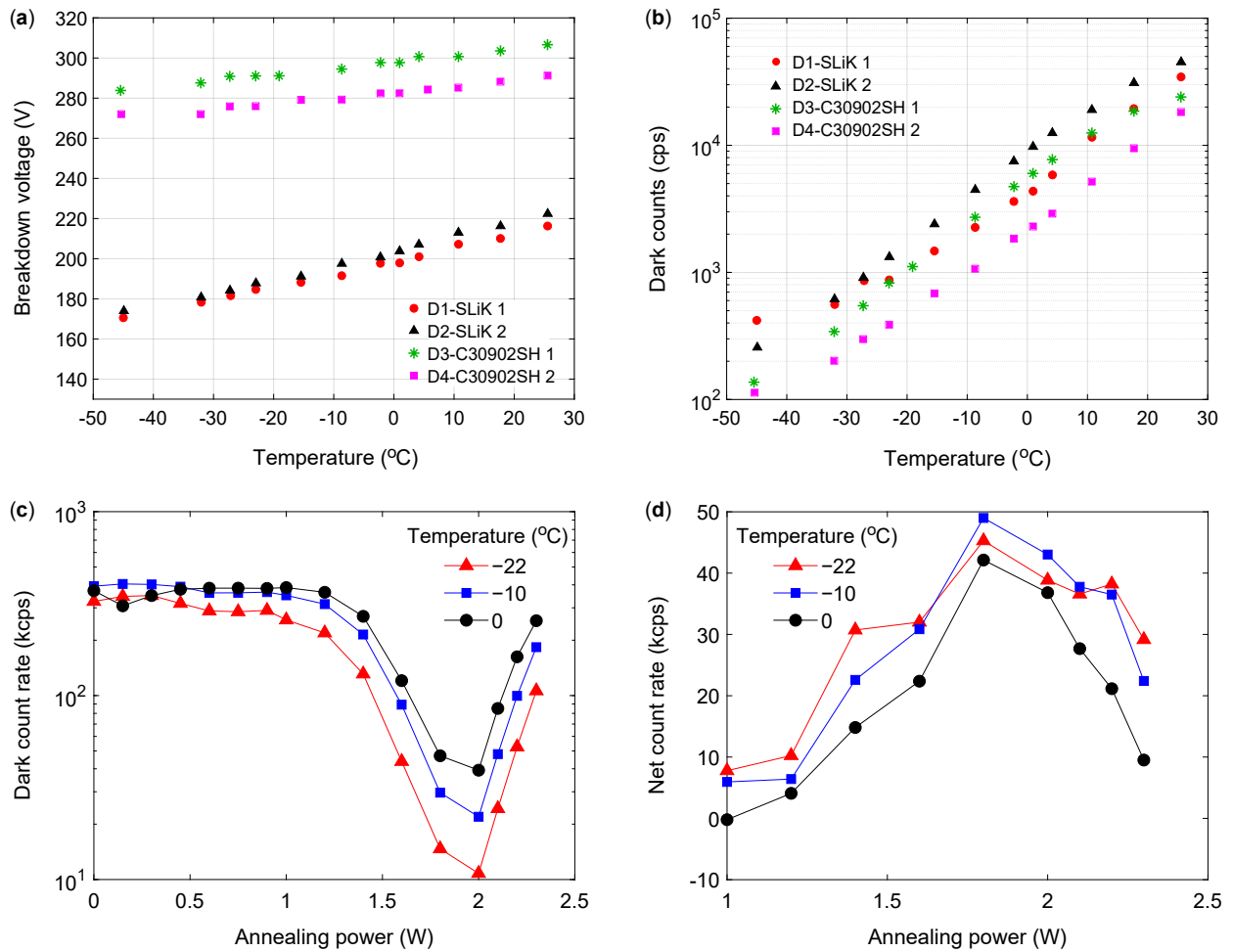


FIG. 5. Results of performance tests. (a) Breakdown voltage and (b) dark count rate of SPADs in the flight annealing payload across the temperature range. (c,d) Data from TVAC testing of the engineering module, showing (c) measured dark count rate and (d) net count rate of an irradiated SPAD after its annealing with increasing powers. Plot (c) and -22°C data in (d) are reprinted from [28].

model of the CAPSat SPAD module that included all new detector samples. The breakdown voltages and DCR of the four SPADs were measured, see Fig. 5(a,b). The SLiK devices (D1 and D2) have lower breakdown voltages in comparison to the C30902SH samples (D3 and D4). The breakdown voltage for SLiK (C30902SH) devices varied by approximately $0.6\text{ V}^\circ\text{C}^{-1}$ ($0.3\text{ V}^\circ\text{C}^{-1}$). As temperature increased, the DCR of the detectors increased exponentially up to tens of kilocounts per second when biased at 20 V excess bias [Fig. 5(b)].

Post-radiation SPAD performance test: This test was conducted inside a thermal vacuum chamber at a pressure of 10^{-6} Torr on an engineering model (EM) of the SPAD module. This EM module is equivalent to the flight module but utilizes four pre-irradiated SLiK detectors, each subjected to a ten-year equivalent low Earth orbit proton dose of 2×10^{10} protons/cm², as reported in [31]. This test was performed to verify the expected behaviour of this module in a space environment. All four detectors underwent laser annealing at vacuum pressure,

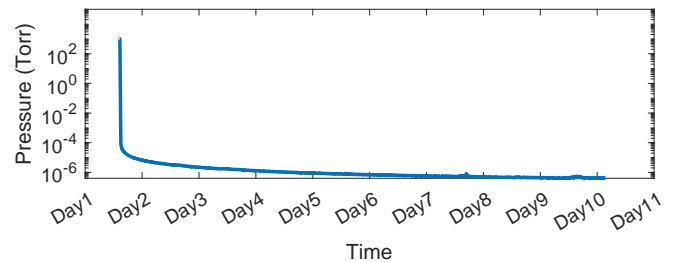


FIG. 6. Observed pressure inside TVAC chamber over 10 days of the SPAD module operation.

utilizing optical power from a laser diode located outside the TVAC chamber. Detailed test procedures and protocols are described in [28]. This test demonstrated that high annealing power applied for a short duration can effectively reduce the dark counts. For instance, Fig. 5(c,d) illustrates that optical power ranging from 1 W to 2 W for

TABLE I. Key features of the SPAD module in TVAC testing

Size	$90 \times 90 \times 52 \text{ mm}^3$
Mass	250 g
Component grade	Mostly automotive or industrial
Power consumption	0.02 W in quiescent mode 0.93 W with SPAD at $4^\circ\text{C}^{\text{a}}$ 1.28 W with SPAD at $-23^\circ\text{C}^{\text{a}}$
Maximum temperature increase ^b	4.56 °C (detector aluminum mount) 4.12 °C (high-voltage supply) 4.69 °C (bottom of PCB)

^a Measured at room temperature, with only one detector and one TEC running at a time.

^b During ~ 1 h of operation under vacuum.

180 s improved both the dark count rates and net count rates (the difference between the count rates with and without light). For more annealing results, see [28].

Engineering performance of the module: Key features of this module are provided in Table I. Its total power consumption is under 1.3 W, well below the CAPSat requirement of 2 W. During TVAC testing, no noticeable outgassing events were observed, as shown in (Fig. 6). Continuous temperature monitoring was conducted at three locations on the SPAD module: the aluminum mount, one of the high voltage supplies, and the bottom of the PCB during repeated annealing and subsequent operation of the module. The highest recorded temperature was 5°C above ambient at the aluminum

mount, with no significant temperature fluctuations observed during extended SPAD operation inside vacuum, demonstrating its capability to function effectively in a vacuum environment.

IV. CONCLUSION

We presented a detailed design and implementation of the detector module, which was specifically engineered to function efficiently in the low-power and low-mass environment typical of CubeSats. We have also explained the concept of in-orbit operation of the detector module. We have completed its ground tests in preparation to implementing laser annealing on SPADs in space. The design of our detector module has been adapted for the upcoming Space Entanglement and Annealing QUantum Experiment (SEAQUE) [27], which will demonstrate the in-orbit annealing along with an entangled photon source, showcasing the potential advancement of space-based SPAD technology.

ACKNOWLEDGEMENTS

We thank Excelitas Technologies for discussions, customising their device package, and providing selected SPAD samples. This work is funded by the Canada Foundation for Innovation (CFI), the Canadian Space Agency (CSA), the Ontario Research Fund (ORF), the Natural Sciences and Engineering Research Council of Canada (NSERC), and Industry Canada.

-
- [1] Liao, Sheng-Kai, Cai, Wen-Qi, Liu, Wei-Yue, Zhang, Liang, Li, Yang, Ren, Ji-Gang, Yin, Juan, Shen, Qi, Cao, Yuan, Li, Zheng-Ping, and others. *Satellite-to-ground quantum key distribution*. Nature, 549(7670):43, 2017. Nature Publishing Group.
 - [2] Yin, Juan, Cao, Yuan, Li, Yu-Huai, Liao, Sheng-Kai, Zhang, Liang, Ren, Ji-Gang, Cai, Wen-Qi, Liu, Wei-Yue, Li, Bo, Dai, Hui, and others. *Satellite-based entanglement distribution over 1200 kilometers*. Science, 356(6343):1140–1144, 2017. American Association for the Advancement of Science.
 - [3] Ren, Ji-Gang, Xu, Ping, Yong, Hai-Lin, Zhang, Liang, Liao, Sheng-Kai, Yin, Juan, Liu, Wei-Yue, Cai, Wen-Qi, Yang, Meng, Li, Li, and others. *Ground-to-satellite quantum teleportation*. Nature, 549(7670):70, 2017. Nature Publishing Group.
 - [4] Liao, Sheng-Kai, Cai, Wen-Qi, Handsteiner, Johannes, Liu, Bo, Yin, Juan, Zhang, Liang, Rauch, Dominik, Fink, Matthias, Ren, Ji-Gang, Liu, Wei-Yue, and others. *Satellite-relayed intercontinental quantum network*. Physical Review Letters, 120(3):030501, 2018. APS.
 - [5] Takenaka, Hideki, Carrasco-Casado, Alberto, Fujiwara, Mikio, Kitamura, Mitsuo, Sasaki, Masahide, and Toyoshima, Morio. *Satellite-to-ground quantum-limited communication using a 50-kg-class microsatellite*. Nature Photonics, 11(8):502, 2017. Nature Publishing Group.
 - [6] Günthner, Kevin, Khan, Imran, Elser, Dominique, Stiller, Birgit, Bayraktar, Ömer, Müller, Christian R., Saucke, Karen, Tröndle, Daniel, Heine, Frank, Seel, Stefan, and others. *Quantum-limited measurements of optical signals from a geostationary satellite*. Optica, 4(6):611–616, 2017. Optical Society of America.
 - [7] Yang, Meng, Xu, Feihu, Ren, Ji-Gang, Yin, Juan, Li, Yang, Cao, Yuan, Shen, Qi, Yong, Hai-Lin, Zhang, Liang, Liao, Sheng-Kai, and others. *Spaceborne, low-noise, single-photon detection for satellite-based quantum communications*. Optics Express, 27(25):36114–36128, 2019. Optical Society of America.
 - [8] Bourgoïn, J. P., Meyer-Scott, E., Higgins, Brendon L., Helou, B., Erven, Chris, Huebel, Hannes, Kumar, B., Hudson, D., D’Souza, Ian, Girard, Ralph, and others. *A comprehensive design and performance analysis of low Earth orbit satellite quantum communication*. New Journal of Physics, 15(2):023006, 2013. IOP Publishing.
 - [9] Bourgoïn, Jean-Philippe, Gigov, Nikolay, Higgins, Brendon L., Yan, Zhizhong, Meyer-Scott, Evan, Khandani, Amir K., Lütkenhaus, Norbert, and Jennewein, Thomas. *Experimental quantum key distribution with simulated*

- ground-to-satellite photon losses and processing limitations*. Physical Review A, 92(5):052339, 2015. APS.
- [10] Sun, Xiaoli, Krainak, Michael A., Abshire, James B., Spinhirne, James D., Trottier, Claude, Davies, Murray, Dautet, Henri, Allan, Graham R., Lukemire, Alan T., and Vandiver, James C. *Space-qualified silicon avalanche-photodiode single-photon-counting modules*. Journal of Modern Optics, 51(9-10):1333–1350, 2004. Taylor & Francis.
- [11] Sun, Xiaoli, Jester, Peggy L., Palm, Stephen P., Abshire, James B., Spinhirne, James D., and Krainak, Michael A. *In orbit performance of Si avalanche photodiode single photon counting modules (SPCM) used in the Geoscience Laser Altimeter System on ICESat*. Proc. SPIE, 6372:63720P, 2006.
- [12] Sun, Xiaoli, Jester, Peggy L., Abshire, James B., and Chang, Edward S. *Performance of the GLAS space lidar receiver through its seven-year space mission*. In CLEO: Applications and Technology, pages ATuA2, 2011. Optical Society of America.
- [13] Schutz, Bob E., Zwally, H. Jay, Shuman, Christopher A., Hancock, D., and DiMarzio, John P. *Overview of the ICESat mission*. Geophysical Research Letters, 32:L21S01, 2005.
- [14] Bennett, C. H. and Brassard, G. *Quantum Cryptography: Public Key Distribution and Coin Tossing*. In Proc. International Conference on Computers, Systems, and Signal Processing, pages 175-179, 1984. IEEE Press, New York.
- [15] Ekert, A.K. *Quantum cryptography based on Bell's theorem*. Physical Review Letters, 67(6):661, 1991. APS.
- [16] Bennett, Charles H., Brassard, Gilles, Crépeau, Claude, Jozsa, Richard, Peres, Asher, and Wootters, William K. *Teleporting an unknown quantum state via dual classical and Einstein-Podolsky-Rosen channels*. Physical Review Letters, 70(13):1895, 1993. APS.
- [17] Sun, Xiaoli, Reusser, Daniel, Dautet, Henri, and Abshire, James B. *Measurement of proton radiation damage to Si avalanche photodiodes*. IEEE Transactions on Electron Devices, 44(12):2160–2166, 1997. IEEE.
- [18] Tan, Yue Chuan, Chandrasekara, Rakhitha, Cheng, Cliff, and Ling, Alexander. *Silicon avalanche photodiode operation and lifetime analysis for small satellites*. Optics Express, 21(14):16946–16954, 2013. Optical Society of America.
- [19] Sun, Xiaoli and Dautet, Henri. *Proton radiation damage of Si APD single photon counters*. In Proc. Radiation Effects Data Workshop, pages 146-150, 2001. IEEE.
- [20] Marisaldi, Martino, Maccagnani, Piera, Moscatelli, Francesco, Labanti, Claudio, Fuschino, Fabio, Prest, Michela, Berra, Alessandro, Bolognini, Davide, Ghioni, Massimo, Rech, Ivan, and others. *Single photon avalanche diodes for space applications*. In 2011 IEEE Nuclear Science Symposium Conference Record, pages 129–134, 2011. IEEE.
- [21] Prochazka, Ivan, Hamal, Karel, and Král, Lucas. *Single photon counting module for space applications*. Journal of Modern Optics, 54(2-3):151–161, 2007. Taylor & Francis.
- [22] Moscatelli, Francesco, Marisaldi, Martino, Maccagnani, Piera, Labanti, Claudio, Fuschino, Fabio, Prest, Michela, Berra, Alessandro, Bolognini, Davide, Ghioni, Massimo, Rech, Ivan, and others. *Radiation tests of single photon avalanche diode for space applications*. Nuclear Instruments and Methods in Physics Research A, 711:65-72, 2013. Elsevier.
- [23] Anisimova, Elena, Higgins, Brendon L., Bourgoïn, Jean-Philippe, Cranmer, Miles, Choi, Eric, Hudson, Danya, Piche, Louis P., Scott, Alan, Makarov, Vadim, and Jennewein, Thomas. *Mitigating radiation damage of single photon detectors for space applications*. EPJ Quantum Technology, 4(1):10, 2017. Springer.
- [24] Lim, Jin Gyu, Anisimova, Elena, Higgins, Brendon L., Bourgoïn, Jean-Philippe, Jennewein, Thomas, and Makarov, Vadim. *Laser annealing heals radiation damage in avalanche photodiodes*. EPJ Quantum Technology, 4(1):11, 2017. SpringerOpen.
- [25] Bugge, Audun Nystad, Sauge, Sebastien, Ghazali, Aina Mardhiyah M, Skaar, Johannes, Lydersen, Lars, and Makarov, Vadim. *Laser damage helps the eavesdropper in quantum cryptography*. Physical Review Letters, 112(7):070503, 2014. APS.
- [26] Siv Schwink. *Self-annealing photon detector brings global quantum internet one step closer to feasibility*. 2021. Available online: <https://physics.illinois.edu/news/CAPSat-in-orbit>.
- [27] Jet Propulsion Laboratory. *SEAQUE: Space Station to Host "Self-Healing" Quantum Communications Technology Demo*. 2022. Available online: <https://scitechdaily.com/seaque-space-station-to-host-self-healing-quantum-communications-technology-demo/>.
- [28] Krynski, Joanna, Sultana, Nigar, Lee, Youn Seok, Makarov, Vadim, and Jennewein, Thomas. *Protocols for healing radiation-damaged single-photon detectors suitable for space environment*. IEEE Transactions on Nuclear Science, 2023. IEEE.
- [29] Haitz, Roland H. *Mechanisms contributing to the noise pulse rate of avalanche diodes*. Journal of Applied Physics, 36(10):3123–3131, 1965. AIP.
- [30] Cova, S., Ghioni, M., Lacaita, A., Samori, C., and Zappa, F. *Avalanche photodiodes and quenching circuits for single-photon detection*. Applied Optics, 35(12):1956–1976, 1996. Optical Society of America.
- [31] DSouza, Ian, Bourgoïn, Jean-Philippe, Higgins, Brendon L., Lim, Jin Gyu, Tannous, Ramy, Agne, Sascha, Moffat, Brian, Makarov, Vadim, and Jennewein, Thomas. *Repeated radiation damage and thermal annealing of avalanche photodiodes*. EPJ Quantum Technology, 8(1):13, 2021. Springer Berlin Heidelberg.